Nanoelectronics and Its New Materials – A NEW ERA OF NANOSCIENCE

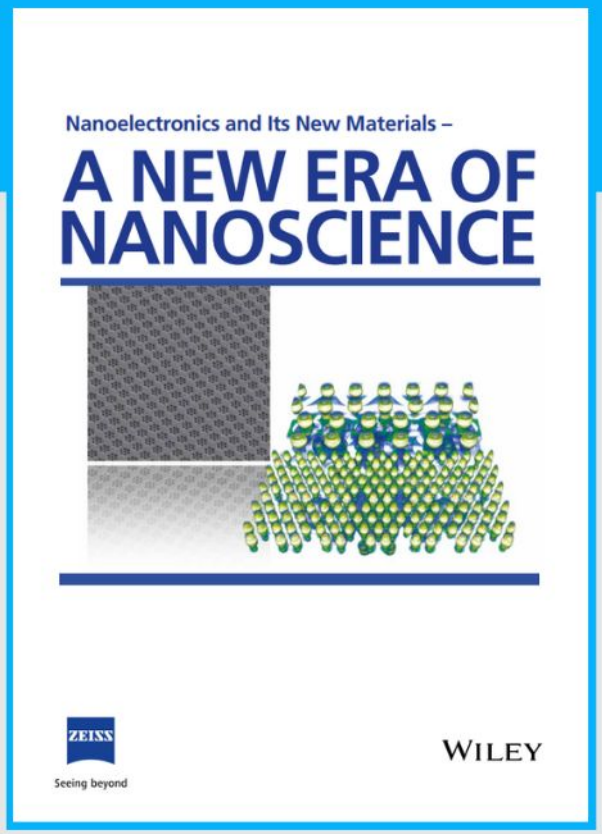

Discover the recent advances in electronics research and fundamental nanoscience.

Nanotechnology has become the driving force behind breakthroughs in engineering, materials science, physics, chemistry, and biological sciences. In this compendium, we delve into a wide range of novel applications that highlight recent advances in electronics research and fundamental nanoscience. From surface analysis and defect detection to tailored optical functionality and transparent nanowire electrodes, this eBook covers key topics that will revolutionize the future of electronics.

To get your hands on this valuable resource and unleash the power of nanotechnology, simply download the eBook now. Stay ahead of the curve and embrace the future of electronics with nanoscience as your guide.

ZEISS

Seeing beyond

WILEY

ADVANCED FUNCTIONAL MATERIALS
www.afm-journal.de

Introducing MR-TADF Emitters into Light-Emitting Electrochemical Cells for Narrowband and Efficient Emission

Shi Tang, John Marques dos Santos, Joan Ràfols-Ribé, Jia Wang, Eli Zysman-Colman, and Ludvig Edman**

Organic semiconductors that emit by the process of multi-resonance thermally activated delayed fluorescence (MR-TADF) can deliver narrowband and efficient electroluminescence while being processable from solvents and metal-free. This renders them attractive for use as the emitter in sustainable light-emitting electrochemical cells (LECs), but so far reports of narrowband and efficient MR-TADF emission from LEC devices are absent. Here, this issue is addressed through careful and systematic material selection and device development. Specifically, the authors show that the detrimental aggregation tendency of an archetypal rigid and planar carbazole-based MR-TADF emitter can be inhibited by its dispersion into a compatible carbazole-based blend host and an ionic-liquid electrolyte, and it is further demonstrated that the tuning of this active material results in a desired balanced p- and n-type electrochemical doping, a high solid-state photoluminescence quantum yield of 91%, and singlet and triplet trapping on the MR-TADF guest emitter. The introduction of this designed metal-free active MR-TADF material into a LEC, employing air-stabile electrodes, results in bright blue electroluminescence of 500 cd m^{-2}, which is delivered at a high external quantum efficiency of 3.8% and shows a narrow emission profile with a full-width-at-half-maximum of 31 nm.

1. Introduction

The discovery and development of organic semiconductors that emit by the process of thermally activated delayed fluorescence (TADF) was paradigm shifting since such compounds can harvest both triplets and singlet excitons for the generation of efficient electroluminescence while being free from expensive and scarce metals.[1] This first generation of TADF emitters exhibited very broad emission spectra, with a typical full width at half maximum (FWHM) of 70–100 nm[2] because of significant structural motions in the emissive first excited singlet state (S_1) and a strong vibronic coupling between S_1 and the singlet ground state (S_0). Such a broad emission spectrum is an undesirable feature for applications where a pure color or a distinct emission wavelength is desired, for example, full-color displays[3] and light-treatment devices.[4]

In this context, the contributions from Hatakeyama and co-workers of organic semiconductors that deliver efficient and narrowband electroluminescence by a process and materials design termed multi-resonance TADF (MR-TADF) are noteworthy.[5] An MR-TADF emitter is typically a rigid heteroatom-doped nanographene, with its HOMO and LUMO localized on adjacent atoms.[6] This type of spatial separation of the frontier orbitals can result in short-range charge-transfer excited states that possess a small energy gap between the first excited triplet state (T_1) and S_1 (ΔE_{ST}), which in turn results in that the triplet excitons can be thermally upconverted to the emissive S_1 state at ambient temperature by reverse intersystem crossing (RISC). Simultaneously, the molecular rigidity of typical MR-TADF compounds suppresses structural relaxations in the S_1 state and weakens the vibronic coupling between the S_1 and S_0 states resulting in narrowband emission.

The practical relevance of MR-TADF compounds was first demonstrated in vacuum-processed organic light-emitting diodes (OLEDs), which showed high maximum external quantum efficiency (EQE_{max}) that can even exceed 40%[7] and an extremely narrow FWHM that can be less than 20 nm.[8] For many applications, device fabrication by printing and coating is preferred because it can be more cost-effective and sustainable

S. Tang, J. Ràfols-Ribé, J. Wang, L. Edman
The Organic Photonics and Electronics Group
Department of Physics
Umeå University
Umeå SE-90187, Sweden
E-mail: ludvig.edman@umu.se

J. M. dos Santos, E. Zysman-Colman
Organic Semiconductor Centre
EaStCHEM School of Chemistry
University of St Andrews
St Andrews KY16 9ST, UK
E-mail: eli.zysman-colman@st-andrews.ac.uk

The ORCID identification number(s) for the author(s) of this article can be found under https://doi.org/10.1002/adfm.202306170

DOI: 10.1002/adfm.202306170

than by vacuum deposition.[9] Although the characteristic rigid molecular structure of MR-TADF compounds can pose challenges in this context, for instance in regards to their solubility in common ink solvents, a number of recent reports[10] have shown that OLEDs using solution-processable MR-TADF compounds can deliver high EQE and narrowband electroluminescence. However, the more generic problem with OLEDs is that they commonly comprise a multitude of highly exact thin organic semiconductor layers, which render their complete printing and coating fabrication challenging.

The light-emitting electrochemical cell (LEC) is an alternative emissive thin-film device technology,[11] which is similar in appearance to the OLED, but is distinguished by its much simpler and robust device structure that facilitates for a demonstrated printing and coating fabrication of complete LEC devices under ambient air.[9a,c,12] This fabrication opportunity is enabled by the existence of mobile ions in the active material, which redistribute in a complex manner for the in situ formation of a p-n junction during the initial LEC operation.[13] A number of reports on the employment of TADF emitters in LEC devices can be found in the scientific literature, and although these devices, in some cases, deliver promising emission efficiency, they also invariably feature broad emission spectra.[14] Karaman et al. recently reported on the synthesis of two cationic MR-TADF compounds, which comprised a DiKTa[15] core endowed with a chemically grafted imidazolium cation that is charge-compensated by a mobile PF_6^- anion.[16] They introduced a neat thin film of one, or a blend, of these two ionic compounds as the active material in an LEC device, which produced electroluminescence. The drawbacks were that the peak luminance and the EQE were modest at 15 cd m^{-2} and <0.01%, respectively, and notably that the emission spectrum was broad with a FWHM of >100 nm.[16]

Here, we report on the development of the first MR-TADF LEC that delivers bright and narrowband emission at 500 cd m^{-2} and a FWHM of 31 nm, respectively, at a high EQE_{max} of 3.8%. The peak emission wavelength of the blue-emitting MR-TADF LEC is 489 nm and the CIE coordinates are (0.11, 0.35). The carefully tuned active material comprises a neutral carbazole-based MR-TADF emitter and an ionic liquid dispersed into a carbazole-based majority blend host. The concept-demonstrating device performance was enabled by the systematic design and tuning of the solution-processed host:guest active-material film, which exhibits significant electrochemical p-type and n-type doping capacity for both the host and guest compounds, efficient host-to-guest-transfer of both singlet and triplet excitons, a high solid-state photoluminescence quantum yield (PLQY) of 91%, and similarly sized traps for electron and hole transport.

2. Results and Discussion

Figure 1a shows the molecular structure of the employed MR-TADF emitter: a boron- and nitrogen-containing nanographene termed 2,6-bis(3,6-di-*tert*-butyl-9*H*-carbazol-9-yl)boron (DtBuCzB).[17] The four flexible and hydrophobic *tert*-butyl substituents on the two carbazole units impart a desired high solubility of the otherwise rigid molecule in common organic solvents, as exemplified by a measured high solubility of 40 g L^{-1} in chlorobenzene. DtBuCzB was synthesized according to a protocol from the literature,[17] and its molecular structure and purity were verified with a combination of ^{1}H NMR and ^{13}C NMR spectroscopy and high-performance liquid chromatography (HPLC) (Figures S1–S3, Supporting Information).

Figure 1b displays the absorption spectrum (dashed black line) and the PL spectrum (solid black line) of a dilute chlorobenzene solution of DtBuCzB ([1×10^{-5} M]), as well as the PL spectrum of a neat DtBuCzB film (solid red line). The corresponding values for the PLQY and the FWHM of the PL spectrum ($FWHM_{PL}$) are presented in the inset. The solution of DtBuCzB in chlorobenzene exhibits very sharp and narrowband absorption and PL spectra ($FWHM_{abs}$ = 24 nm, $FWHM_{PL}$ = 25 nm), a high PLQY of 92%, and a very small Stokes shift (i.e., the difference between the absorption and PL peaks) of 20 nm.

This set of photophysical features is in agreement with monomolecular MR-TADF emission. The optically active conjugated core structure of DtBuCzB is very rigid and therefore remains essentially invariant during the S_0-S_1 transition. This is reflected in the narrowband absorption and PL spectra and the small Stokes shift. The same rigidity of the core structure also suppresses the nonradiative deactivation of the excited state, which is a prerequisite for a high PLQY.

The transfer of DtBuCzB into a neat solid film results in a red-shifted PL spectrum (compare solid black line with dashed red line in Figure 1b), a marked broadening of the $FWHM_{PL}$ from 25 to 60 nm, and a significant lowering of the PLQY from 92% to 22%. This behavior is rationalized by the propensity of the rigid and flat DtBuCzB molecules to aggregate and that these aggregates in the neat film form poorly emissive excimers with a lowered energy gap.[18] A functional solution to this type of undesired emitter aggregation in the active material of electroluminescent devices is to disperse the emitter into a second compatible majority "host" organic semiconductor, which also can perform the duty of electronic transport.

Figure 1c shows the molecular structure of two identified prospective host compounds: 2,6-di(9*H*-carbazol-9-yl)pyridine (PYD2Cz) and 2,6-bis(3-(carbazol-9-yl)phenyl)pyridine (26DCzPPy). Their selection was based on three different criteria: i) they comprise (two) carbazole units to render them compatible with the carbazole-based DtBuCzB guest compound (see Figure 1a), so that the minority guest can be well dispersed into the majority host matrix in the solid state[14h]; ii) they feature high solubility in common hydrophobic solvents, notably 40 g L^{-1} in chlorobenzene, so that the host:guest blend can be solution-processed into uniform thin films; iii) they both feature higher triplet energy than that of the DtBuCzB guest emitter to enable facile host-to-guest Dexter energy transfer and efficient guest emission (see Figure 1d).[17,19]

Figure 1e presents the PL spectra of thin films of the PYD2Cz single host (solid black squares), the 26DCzPPy single host (open blue circles), and the PYD2Cz:26DCzPPy blend host (mass ratio = 50:50, solid red triangles). The observation that the PL spectrum of the PYD2Cz:26DCzPPy blend host (PL_{peak} = 386 nm) is a superposition of, and not red shifted with respect to, the PL spectra of the PYD2Cz single host (PL_{peak} = 375 nm) and the 26DCzPPy single host (PL_{peak} = 390 nm) suggests that the blend host does not form exciplexes. Figure 1e also shows the absorption spectrum of the dilute DtBuCzB-in-chlorobenzene solution (dashed black line).

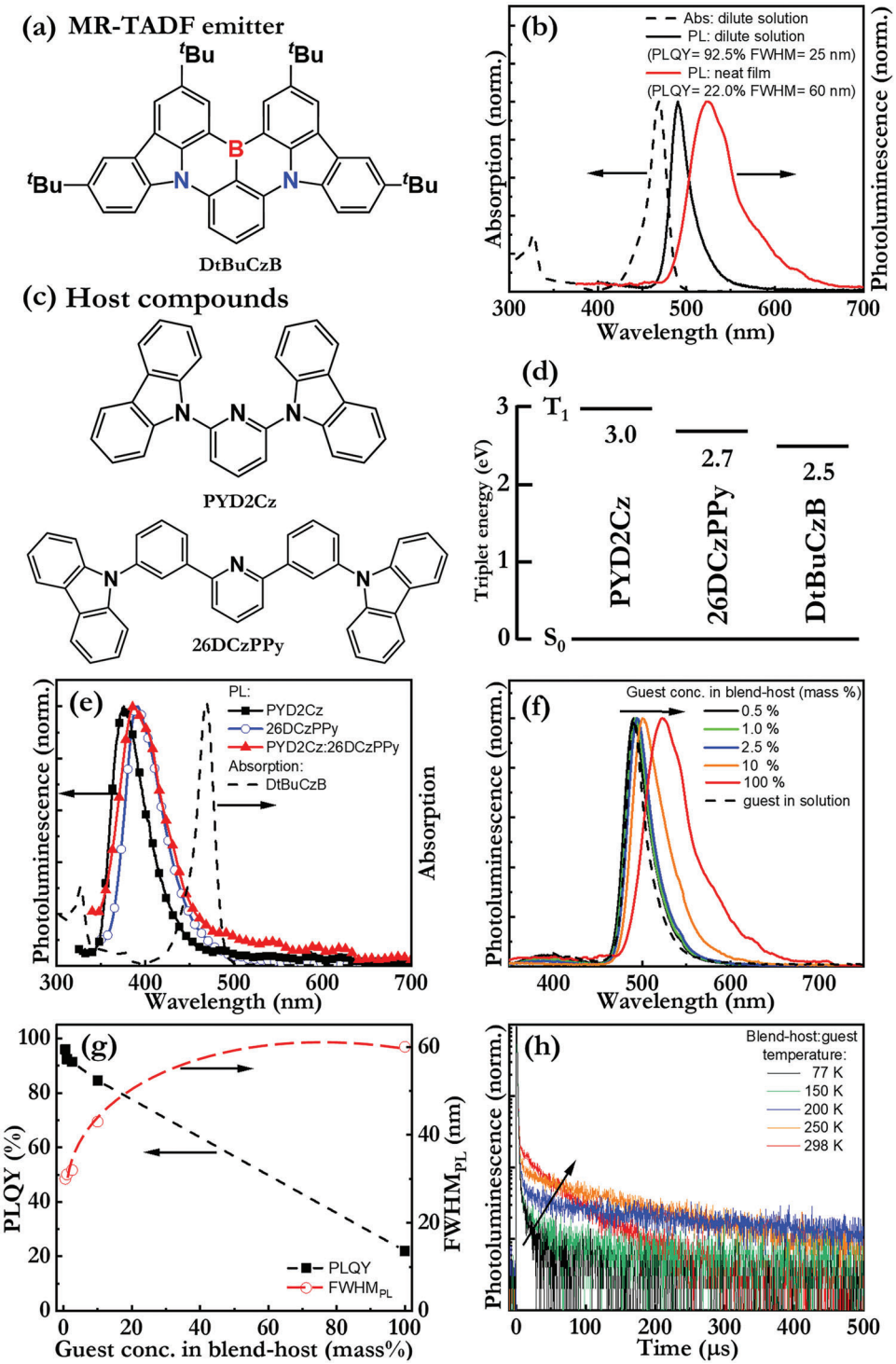

Figure 1. a) The molecular structure of the DtBuCzB emitter. b) The absorption spectrum (dashed black line, left *y*-axis) and the PL spectrum (solid black line, right *y*-axis) of DtBuCzB in dilute chlorobenzene solution. The DtBuCzB solute concentration is 1×10^{-5} M. The PL spectrum of a DtBuCzB neat film is presented by the solid red line. The corresponding values for the PLQY and the FWHM are presented in the inset. c) The molecular structure of the two host compounds: PYD2Cz and 26DCzPPy. d) The triplet energies of the host and guest compounds. e) The PL spectra of thin films of the neat host compounds and the blend host (solid lines), and the absorption spectrum of the dilute DtBuCzB-in-chlorobenzene solution (dashed black line). f) The PL spectrum of the blend-host:guest film as a function of the DtBuCzB guest concentration, with the arrow indicating increasing guest concentration. The PL spectrum of the dilute DtBuCzB-in-chlorobenzene solution is included as a reference (dashed black line). g) The PLQY (left *y*-axis) and the FWHM of the PL spectrum (right *y*-axis) of the blend-host:guest film as a function of guest concentration. h) The temperature-dependent PL intensity transients of the blend-host:guest film, with the arrow indicating increasing temperature. All spectra were normalized to the peak intensity value.

The evolution of the PL spectrum of the blend-host:guest film with increasing guest concentration is depicted in Figure 1f, with the arrow indicating increasing DtBuCzB guest concentration. The PL spectrum of the dilute DtBuCzB guest emitter in chlorobenzene solution (dashed black line) is included as a reference of well-dispersed guest behavior. The associated changes in the PLQY and $FWHM_{PL}$ with increasing guest concentration are shown in Figure 1g, while Figure S4, Supporting Information, and **Table 1** show the corresponding spectra and data for the two single-host:guest systems. We first note that the absence of host emission (at ≈390 nm, see Figure 1e) implies that the host-to-guest energy transfer is complete in all investigated host:guest films, although the overlap between the PL spectrum of the host and the absorption spectrum of the dispersed DtBuCzB guest is moderate (see Figure 1e). We further call attention to the fact that all of the solid host:guest films with a guest concentration of ≤2.5 mass% feature narrowband and efficient PL, with a $FWHM_{PL}$ of ≈30 nm and a PLQY >90%. The conclusion is thus that the three carbazole-based host systems are capable of suppressing the aggregation of the DtBuCzB guest emitter up to a guest concentration of 2.5 mass%.

Table 1 further shows that the PLQY is consistently markedly higher under inert N_2 atmosphere than under ambient air. This observation is in line with the fact that a significant fraction of the photoexcited singlet excitons are converted to the triplet state by intersystem crossing (ISC), where they are quenched by O_2 molecules (if present), before being back-converted to the emissive singlet state by RISC. This type of ISC/RISC loop, as manifested in a distinctly lower PLQY under air than under inert N_2, is a well-documented characteristic of a TADF emitter.[20] The TADF capacity of the solid blend-host:guest film was further verified by the temperature-dependent PL transients, depicted in Figure 1h. The PL transients are found to essentially comprise two components, one fast component with a radiative lifetime of 6.6 ns, and one slow component with a radiative lifetime of 39 µs, and the intensity of the slow transient was observed to increase with temperature, as indicated by the arrow. This temperature-induced increase of the slow component is assigned to a thermally activated upconversion of excitons from the nonemissive T_1 state to the emissive S_1 state by RISC, which corroborates the TADF nature of the emission of DtBuCzB in the host environment.

The functional operation of a LEC is dependent on that the organic semiconductor(s) in the active material can be electrochemically p-type and n-type doped. This in situ doping capacity can conveniently be evaluated by cyclic voltammetry (CV). **Figure 2**a–c presents CV traces recorded of the DtBuCzB emitter (Figure 2a), the PYD2Cz single host (Figure 2b), and the 26DCzPPy single host (Figure 2c) in both dilute DMF solution (dashed black line) and as a neat film (solid red line). The CV traces feature partially reversible oxidation and reduction reactions, which we assign to electrochemical p-type doping and n-type doping, respectively, of the investigated organic semiconductor, in line with earlier literature.[14h,17,21]

The onset potentials for the electrochemical doping reactions were established with the procedure detailed in the Experimental Section, and the derived onset potentials are indicated by the vertical dotted lines in Figure 2a–c. These onset potentials (vs the Fc/Fc^+ reference potential, $V_{Fc/Fc+}$) can be translated into

Table 1. Summary of key material properties and LEC metrics.

Host	Guest conc. [mass%]	PL_{peak} [nm]	$FWHM_{PL}$ [nm]	PLQY (N_2/air) [%]	EL_{peak} [nm]	$FWHM_{EL}$ [nm]	Turn-on time (> 100 nits) [s]	Peak lumin. [cd m^{-2}]	V_{min} [V]	CE [cd A^{-1}]	EQE [%]	Lifetime [min]
Guest-only	100	521	60	22.0/8.3	515	60	150	120	4.1	1.5	0.52	15
PYD2Cz:	0.5	490	30	96.0/77.4	487	28	40	350	13.3	4.5	2.6	75
26DCzPPy	1	492	31	92.4/78.5	488	30	26	365	13.8	4.7	2.9	175
(50:50 by mass)	2.5	494	32	91.4/79.0	489	31	16	493	14.1	6.3	3.8	180
	10	500	43	84.6/67.8	495	38	3	363	13.2	4.7	2.3	1250
PYD2Cz	1	494	34	99.6/65.2	489	31	—	85	13.1	1.1	0.68	—
	2.5	497	35	99.7/65.2	491	33	80	255	12.5	3.3	2.0	40
	10	500	43	88.9/58.3	496	35	16	145	12.3	1.9	0.92	16
26DCzPPy	1	492	32	98.2/40.7	489	29	195	265	11.8	3.4	2.1	100
	2.5	494	34	97.4/56.3	492	30	12	410	12.6	5.3	3.2	130
	10	498	46	86.7/51.0	494	35	5	325	11.4	4.2	2.1	600

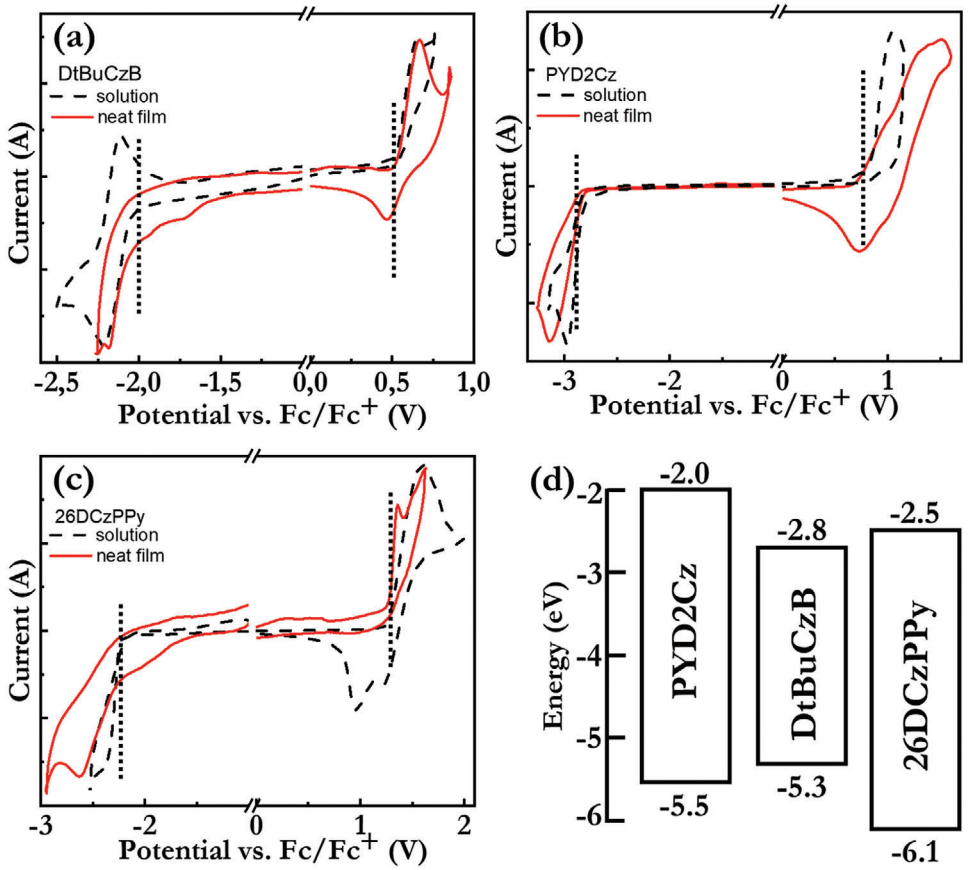

Figure 2. CV traces of a) the MR-TADF guest emitter DtBuCzB, b) the host compound PYD2Cz, and c) the host compound 26DCzPPy, in the form of a neat solid film (solid red line) and as dissolved in DMF solution (dashed black line). The solute concentration in DMF is 1 g L^{-1}, the electrolyte is 0.1 M $THABF_4$, and the scan rate is 0.05 V s^{-1}. The vertical dotted lines indicate the derived onset potentials for electrochemical oxidation and reduction. d) The electron-energy diagram of the host and guest compounds in the LEC active material, as derived from the CV data.

the HOMO and LUMO energies, respectively, with the equation, HOMO/LUMO = $-e\cdot(4.8\,\mathrm{V} + V_{\mathrm{Fc/Fc+}})$, where e is the elementary charge. Figure 2d shows the CV-derived electron-energy diagram for the host:guest systems, which reveals that both the electron and the hole will be trapped on the DtBuCzB guest emitter, regardless of whether PYD2Cz or 26DCzPPy is employed as the single host or PYD2Cz:26DCzPPy is the blend host.

The "trap depth" for electron/hole transport in the host:guest system is defined to be the absolute energy difference between the LUMO/HOMO of the host and the LUMO/HOMO of the guest. It has been shown by combined simulations and experiments that a balanced electron and hole trap depth and a balanced electron and hole mobility of the host will position the emissive p-n junction in the center of the active material of LEC devices,[22] and that such a centered p-n junction can enable highly efficient light emission.[22b,23] Figure 2d shows that the most balanced trap depth is obtained with the blend-host:guest system, which features an electron trap depth of 0.3 eV and a hole trap depth of 0.2 eV.

The LEC devices were fabricated using the following architecture: indium-tin-oxide (ITO)/poly(3,4-ethylenedioxythiophene): poly(styrene sulfonate) (PEDOT:PSS)/active-material/Al (see Figure S5, Supporting Information, for an electron-energy diagram of the device structure). The primary role of the PEDOT:PSS layer is to flatten the ITO surface and, thereby, to suppress the probability for formation of short circuits between the two electrodes. The active material was spin-cast from a chlorobenzene ink, which in addition to the organic semiconductor(s) comprised a tetrahexylammonium tetrafluoroborate ($THABF_4$) ionic liquid as the electrolyte in an optimized concentration of 6.7 mass%. The presented LEC data were recorded on pristine devices, which were driven by a constant current density of 7.7 mA cm^{-2}, with ITO/PEDOT:PSS biased as the positive anode.

Figure 3a,b show the luminance transients (black line, left y-axis) and the voltage transients (red line, right y-axis) for the guest-only LEC and the blend-host:guest LEC, respectively. The latter comprises a PYD2Cz:26DCzPPy:DtBuCzB:$THABF_4$ active material in an optimized mass ratio of 45.4:45.4:2.5:6.7. Table S1, Supporting Information, presents device metrics recorded during the blend-host optimization, whereas Figure 3c,d displays the corresponding luminance and voltage transients for the two single-host:guest LECs. All four different LECs exhibit an increasing luminance and a decreasing voltage during the initial constant-current operation. This behavior is consistent with the fact that the THA cations and BF_4 anions in the active material

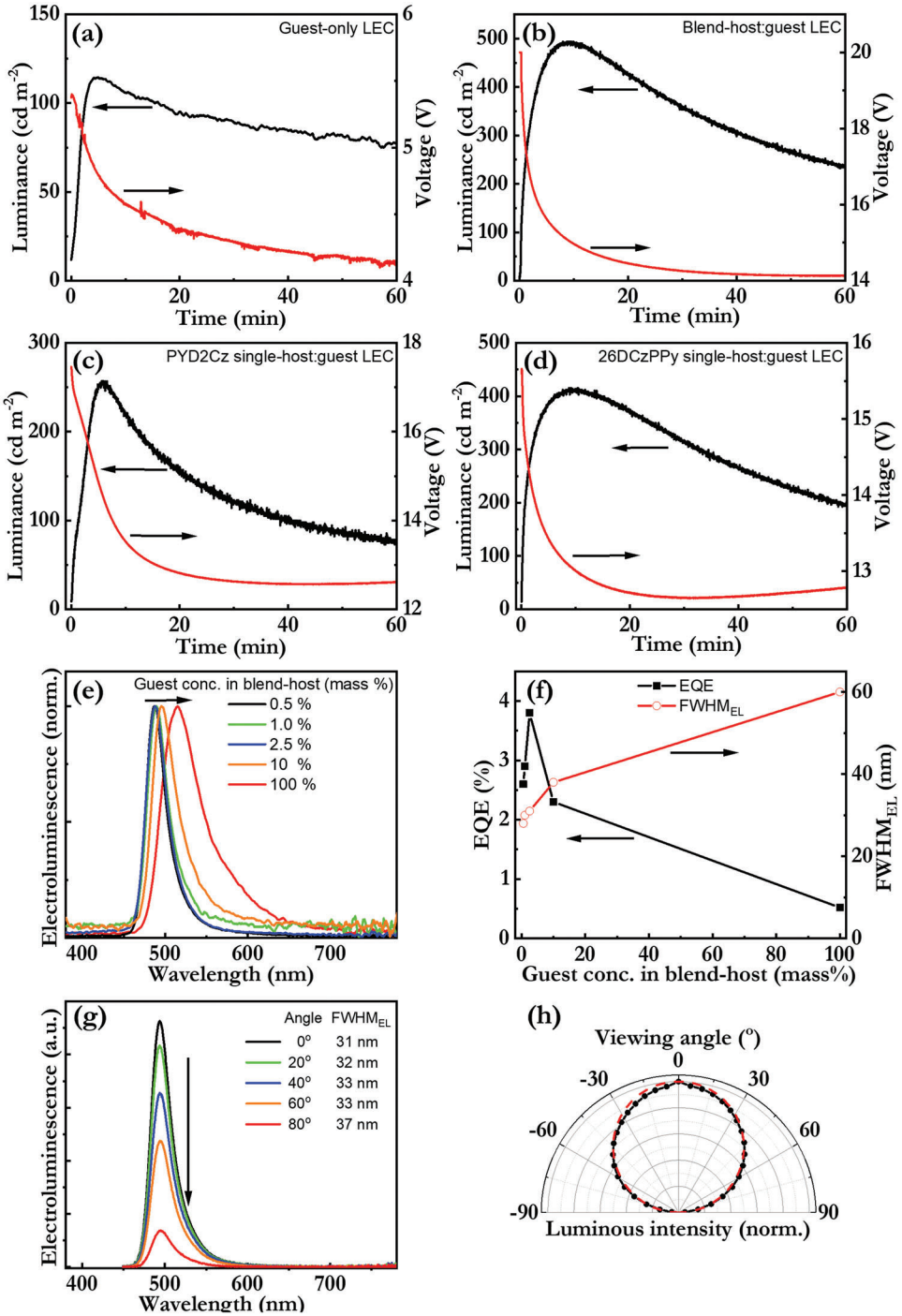

Figure 3. a–d) The temporal evolution of the luminance (black line, left *y*-axis) and the voltage (red line, right *y*-axis) of a) the MR-TADF guest-only LEC, b) the optimized blend-host:guest LEC, c) the PYD2Cz single-host:guest LEC, and d) the 26DCzPPy single-host:guest LEC. e) The steady-state EL spectrum of the blend-host:guest LEC as a function of the guest concentration, with the arrow indicating increasing guest concentration and the inset identifying the absolute value for the guest concentration in the active material. f) The EQE (solid black squares, left *y*-axis) and the FWHM of the EL spectrum (open red circles, right *y*-axis) of the blend-host:guest LEC as a function of guest concentration. g) The steady-state EL spectrum of the optimized blend-host:guest LEC as a function of viewing angle, with the arrow indicating increasing viewing angle and the inset showing the derived values for the FWHM. h) A polar presentation of the steady-state luminous intensity as a function of viewing angle. The red dashed line presents the luminous intensity of an ideal Lambertian emitter. All of the ITO/PEDOT:PSS/active-material/Al LEC devices were driven by a constant current density of 7.7 mA cm^{-2}, and the presented data are from the best performing device out of 4 to 8 investigated. The standard deviation around the mean value (for the peak luminance, the external quantum efficiency, and the operational lifetime) is less than 10%.

are mobile, and, in response to the applied voltage, are first forming injection-facilitating electric double layers at the electrode interfaces, and thereafter enable transport-improving electrochemical doping of the organic semiconductor(s) by electrostatic compensation. The latter process eventually results in the in situ formation of a p-n junction doping structure in the active material, which is concomitant with the fact that the electron and hole recombination to excitons is essentially perfect.[13,24]

The guest-only LEC in Figure 3a features a relatively bright and efficient peak luminance of 120 cd m^{-2} at an EQE of 0.52%, in particular in consideration of its modest solid-state PLQY of 22%. The drawback is that its EL spectrum is markedly broadened ($FWHM_{EL}$ = 60 nm) and red-shifted (EL_{peak} = 515 nm) in comparison to the demonstrated potential for narrowband and blue emission of a well dispersed DtBuCzB emitter (as shown in Figure 1b, solid black line). This implies that the light-emission performance of the guest-only LEC is detrimentally affected by aggregation of the flat and rigid DtBuCzB molecules in the active material, despite the motion of bulky ions during the initial electrochemical doping process.[25]

Importantly, the optimized blend-host:guest LEC, depicted in Figure 3b, delivers a highly appealing LEC performance in the form of simultaneously narrowband, bright, and efficient light emission. More specifically, the presented blend-host:guest LEC device emits blue light, with a narrow $FWHM_{EL}$ of 31 nm, a peak wavelength of 489 nm, and CIE coordinates of (0.11, 0.35), which is delivered at a strong luminance of 493 cd m^{-2} and a high EQE_{max} of 3.8%. The latter corresponds to a respectable current conversion efficacy of 6.3 cd A^{-1}, despite the device being void of outcoupling structures. The dependence of the peak luminance and the EQE_{max} on the driving current density is presented in Figure S6a, Supporting Information. We further note that the turn-on time to a luminance of 100 cd m^{-2} is 16 s for the pristine blend-host:guest LEC device (and that the turn-on time drops radically with increasing current density, see Figure S6b, Supporting Information), which implies that the bulky ionic-liquid ions in the active material are rather mobile.[26]

Figure 3e,f and Table 1 disclose that the sharpest EL spectrum with a $FWHM_{EL}$ of 28 nm is obtained at the lowest guest concentration of 0.5 mass%, but that associated penalties are a sub-optimized EQE of 2.6% and a shortened operational stability (see Table 1). The optimum guest concentration of 2.5 mass% was thus identified as a compromise between the goals of narrow EL spectrum, high emission efficiency, and reasonable operational lifetime. Figure 3g,h further shows that both the emission spectrum and the perceived luminance of the optimized blend-host:guest LEC device, as often desired, are highly invariant of the viewing angle.

However, Figure S7, Supporting Information, presents a combined simulation and measurement study of the angle-dependent EL spectrum of a blend-host:guest LEC equipped with a thicker active material, which establishes that the steady-state p-n junction is positioned close to (in average only ≈17% of the interelectrode gap away from) the Al cathode at steady state. This translates to that the excitons are formed at a distance of 15–30 nm away from the Al cathode in the 120 nm thick devices presented in Figure 3. Such a positioning of the emissive p-n junction next to a metal (Al) electrode is undesirable from an efficiency viewpoint, since metals in general are strong exciton quenchers and since an off-centered p-n junction also will be concomitant with a high concentration of exciton-quenching (electron) polarons in the thin (n-type) doped region in between the p-n junction and the electrode.[27]

This finding suggests that the hole mobility is higher than the electron mobility for the blend host, and that further improvements of the device performance can be achieved with a more balanced host mobility that, in turn, should force a more centered p-n junction.[22b] Finally, the fact that the operational lifetime is observed to increase monotonically with increasing guest concentration up to 10 mass% implies that exciton–exciton quenching interactions are a significant stability-limiting reaction. This observation is also important in that it suggests that a shortening of the emissive lifetime of the MR-TADF guest emitter will provide a route toward an improvement of the device stability and efficiency.

To put our results into perspective, we conclude with a brief summary and discussion of the state-of-the-art in narrowband and efficient emission from LEC devices. The progress in this field has to date primarily been achieved through the utilization of various types of quantum dots as the LEC emitter.[28] Leger and co-workers pioneered the use of CdSe/ZnS core/shell quantum dots in a LEC device, and reported narrowband orange-yellow electroluminescence with a FWHM of 31 nm at a modest EQE of ≈0.1%.[28g] Watkins et al. subsequently employed CdSe/CdS core/shell quantum dots of a wide range of different emission colors as the emissive species in LEC devices, which produced narrowband electroluminescence with a FWHM of 25–39 nm at a respectable current conversion efficacy of 0.4–1.9 cd A^{-1}.[28b] Finally, Slinker and colleagues recently reported a novel procedure for the fabrication of devices that comprise perovskite nanocrystals as the active material sandwiched between a PEDOT:PSS hole injection layer and a LiF electron injection layer, and which featured very narrow FWHM of ≈20 and 18 nm and high EQE_{max} of 8.3% and 4.3% for sky-blue and green devices, respectively.[28c,29] These preceding achievements of narrowband and efficient light emission are both innovative and important, but unfortunately suffer from their reliance on toxic Cd or Pb as critical constituents within the emitting compound. Thus, our contribution that it is possible to simultaneously deliver efficient and narrowband emission from an LEC device comprising a metal-free MR-TADF compound as the emitter is relevant not only from a conceptual viewpoint but also from a sustainability perspective.

3. Conclusions

We report on the rational development and pioneering demonstration of a MR-TADF LEC device that delivers narrowband and efficient light emission. This was achieved by dispersing a carbazole-based MR-TADF emitter and an ionic-liquid electrolyte into a compatible and functional carbazole blend host for the suppression of emitter aggregation and phase separation. The desired result is a metal-free active material that features a high solid-state PLQY, significant and balanced electrochemical doping capacity, and singlet and triplet trapping on the MR-TADF guest emitter. The inclusion of this solution-processed active material in between two air-stabile electrodes enabled the attainment of bright blue electrolumi-

nescence of 500 cd m^{-2} at a high external quantum efficiency of 3.8% and a narrow full-width-at-half-maximum of 31 nm.

4. Experimental Section

The MR-TADF guest emitter DtBuCzB was synthesized according to a literature protocol.[17,30] The ^{1}H and ^{13}C NMR spectra shown in Figures S1 and S2, Supporting Information, were recorded on a Bruker Advance spectrometer (400 MHz for ^{1}H and either and 126 MHz for ^{13}C). The ^{1}H and ^{13}C NMR spectra were referenced with respect to TMS ($\delta = 0$ ppm) and residual solvent peaks. The HPLC analysis shown in Figure S3, Supporting Information, was conducted on a Shimadzu LC-40 HPLC equipped with a Shim-pack GIST 3 µm C18 reverse phase analytical column. The host compounds, 2,6-di(9*H*-carbazol-9-yl)pyridine (PYD2Cz, Lumtec) and 2,6-bis(3-(carbazol-9-yl)phenyl)pyridine (26DCzPPy, Lumtec), and the electrolyte, the ionic liquid tetrahexylammonium tetrafluoroborate ($THABF_4$, Sigma-Aldrich), were used as received. Master solutions were prepared by dissolving each compound separately in chlorobenzene at a concentration of 40 g L^{-1}, and thereafter by stirring the solutions at 70 °C for >6 h on a magnetic hot plate.

The thin films for the optical measurements were spin-coated from the neat or mixed master solutions onto carefully cleaned quartz substrates. The absorption and the photoluminescence (PL) spectra and the PLQY were measured with an integrating sphere connected to a spectrometer (C9920-02G, Hamamatsu Photonics). The PL intensity transients were recorded under vacuum, using a pulsed laser (wavelength = 375 nm, frequency = 500 Hz, pulse width = 100 ns) as the excitation source and a spectrometer (FLS1000, Edinburgh) for the detection. The CV measurement was carried out with a computer-controlled potentiostat (Autolab PGSTAT302, driven by the GPES software). For the film CV, the working electrode comprised the material-under-study drop-cast on a Au-covered glass substrate, while the solution CV used a Pd disc (diameter = 5 mm) as the working electrode. A Pt rod was the counter electrode, a Ag wire was the quasi-reference electrode, and 0.1 M $THABF_4$ (Sigma-Aldrich) in anhydrous CH_3CN (film CV) or dimethylformamide (solution CV) was the electrolyte. Directly after each CV scan, a calibration scan was run with a small amount of ferrocene added to the electrolyte solution. All CV potentials are reported versus the ferrocene/ferrocenium ion (Fc/Fc^{+}) reference potential. The reduction/oxidation onset potentials are defined as the intersection of the baseline with the tangent of the current at its half peak. The CV sample preparation and measurement were performed in a N_2-filled glove box ($[O_2] < 2$ ppm, $[H_2O] < 1$ ppm).

The device fabrication was initiated by a careful cleaning of the indium-tin-oxide (ITO) coated glass substrates (20 Ω sq^{-1}, Thin Film Devices). A poly(3,4-ethylenedioxythiophene):poly(styrene sulfonate) (PEDOT:PSS) ink (Clevios P VP AI 4083, Heraeus) was spin-coated on the ITO at 4000 rpm for 60 s, and the coated film thereafter dried at 120 °C for 30 min. The active-material ink was prepared by blending the master solutions in a desired mass ratio, followed by stirring at 70 °C for >2 h on the magnetic hot plate. The active-material ink was spin-coated on the dry PEDOT:PSS layer at 2000 rpm for 60 s, and the coated film thereafter dried at 70 °C for 2 h. The dry thickness of the PEDOT:PSS and the active-material layers was 40 and 120 nm, respectively, as measured with a profilometer (DekTak XT, Bruker). Finally, a set of 100 nm thick Al cathodes were deposited on top of the active material by thermal vacuum evaporation at $p < 5 \times 10^{-6}$ mbar. The 0.85×0.15 cm^2 emission area was defined by the overlap between the ITO anode and the Al cathode. The LEC devices were measured with a computer-controlled source-measure unit (Agilent U2722A) and a calibrated photodiode, equipped with an eye-response filter (Hamamatsu Photonics), and connected to a data acquisition card (National Instruments USB-6009) via a current-to-voltage amplifier. The EL spectrum was measured with a calibrated spectrometer (USB2000+, Ocean Optics). All of the above presented measurement procedures, with the exception of the deposition of PEDOT:PSS, were carried out in two interconnected N_2-filled glove box ($[O_2] < 2$ ppm, $[H_2O] < 1$ ppm).

The angle-resolved EL intensity and spectrum were measured with a custom-built, automated spectrogoniometer setup. The angle-dependent measurements were conducted under ambient air, and the devices were therefore encapsulated by attaching a 24 × 24 mm^2 glass cover slide (Menzel GmbH, GER) onto the Al cathode side with UV-curable epoxy (E132-60 mL, Ossila). The epoxy was cured by exposure to UV light (λ_{peak} = 365 nm, power density = 80 mW × mm^{-2}, UV-Exposure Box 1, GieTec) for 15 min. The devices were driven by a constant current density of 7.5 mA cm^{-2}.

The optical simulation was performed with the commercial software Setfos (version 5.2, Fluxim AG, Switzerland). The measured and simulated LECs featured an active material thickness of 170 nm. The active material was modeled as a transparent layer with a wavelength- and doping-independent refractive index of $n = 1.8$. The emissive dipoles were simulated by a delta function positioned in the center of p-n junction region. The intrinsic emission spectrum of the emissive dipoles was set equal to the measured PL spectrum of the blend-host:guest film. The position of the emissive dipoles, that is, the center position of the emissive p-n junction, within the active material was determined by minimizing the root mean square error between the simulated and the measured s-polarized angle-dependent EL data, using a previously published procedure.[23]

Statistical Analysis: The photoluminescence and electroluminescence spectra are normalized with respect to the peak intensity. The device performance, as displayed in the figures and as detailed in the tables, are from the best performing device out of 4 to 8 investigated in each category. The standard deviation around the mean value (for the peak luminance, the external quantum efficiency, and the operational lifetime) is less than 10%.

Supporting Information

Supporting Information is available from the Wiley Online Library or from the author.

Acknowledgements

The Umeå University authors wish to acknowledge generous financial support from the Swedish Research Council, the Swedish Energy Agency, Bertil och Britt Svenssons stiftelse för belysningsteknik, Länsstyrelsen Västerbotten, Kempestiftelserna, Olle Engkvists Stiftelse, Wenner-Gren Foundations, and the Wallenberg Initiative Materials Science for Sustainability, WISE. The St Andrews authors thank the Engineering and Physical Sciences Research Council (EP/R035164/1).

Conflict of Interest

The authors declare no conflict of interest.

Data Availability Statement

The research data supporting this publication can be accessed at https://doi.org/10.17630/3b019330-1da3-4c26-9103-5e8b9b9e16c7

Keywords

blue emission, high efficiency, light-emitting electrochemical cells, multi-resonance thermally activated delayed fluorescence, narrowband emission

Received: June 1, 2023
Revised: August 5, 2023
Published online:

[1] a) H. Uoyama, K. Goushi, K. Shizu, H. Nomura, C. Adachi, *Nature* **2012**, *492*, 234; b) D. Zhang, Y. Wada, Q. Wang, H. Dai, T. Fan, G. Meng, J. Wei, Y. Zhang, K. Suzuki, G. Li, L. Duan, H. Kaji, *Adv. Sci.* **2022**, *9*, 2106018.

[2] a) R. Ansari, W. Shao, S.-J. Yoon, J. Kim, J. Kieffer, *ACS Appl. Mater. Interfaces* **2021**, *13*, 28529; b) R. Braveenth, K. Raagulan, Y.-J. Kim, B.-M. Kim, *Mater. Adv.* **2023**, *4*, 374; c) D.-Y. Chen, W. Liu, C.-J. Zheng, K. Wang, F. Li, S. L. Tao, X.-M. Ou, X.-H. Zhang, *ACS Appl. Mater. Interfaces* **2016**, *8*, 16791; d) J.-M. Teng, Y.-F. Wang, C.-F. Chen, *J. Mater. Chem. C* **2020**, *8*, 11340.

[3] H. Cho, C. W. Joo, S. Choi, C.-M. Kang, B.-H. Kwon, J.-W. Shin, K. Kim, D. H. Ahn, N. S. Cho, *Org. Electron.* **2022**, *101*, 106419.

[4] a) A. Wunsch, K. Matuschka, *Photomed Laser Surg* **2014**, *32*, 93; b) J. L. Anderson, C. A. Glod, J. Dai, Y. Cao, S. W. Lockley, *Acta Psychiatr Scand* **2009**, *120*, 203; c) Y. Meesters, W. B. Duijzer, V. Hommes, *J Affect Disord* **2018**, *232*, 48.

[5] T. Hatakeyama, K. Shiren, K. Nakajima, S. Nomura, S. Nakatsuka, K. Kinoshita, J. Ni, Y. Ono, T. Ikuta, *Adv. Mater.* **2016**, *28*, 2777.

[6] a) S. Madayanad Suresh, D. Hall, D. Beljonne, Y. Olivier, E. Zysman-Colman, *Adv. Funct. Mater.* **2020**, *30*, 1908677; b) K. R. Naveen, H. I. Yang, J. H. Kwon, *Commun Chem* **2022**, *5*, 149.

[7] P. Jiang, J. Miao, X. Cao, H. Xia, K. Pan, T. Hua, X. Lv, Z. Huang, Y. Zou, C. Yang, *Adv. Mater.* **2022**, *34*, 2106954.

[8] a) X. Cai, J. Xue, C. Li, B. Liang, A. Ying, Y. Tan, S. Gong, Y. Wang, *Angew. Chem.* **2022**, *134*, e202200337; b) X. Zeng, L. Wang, H. Dai, T. Huang, M. Du, D. Wang, D. Zhang, L. Duan, *Adv. Mater.* **2023**, *32*, 2211316.

[9] a) A. Sandström, L. Edman, *Energy Technol.* **2015**, *3*, 329; b) F. C. Krebs, *Sol. Energy Mater. Sol. Cells* **2009**, *93*, 394; c) J. Zimmermann, L. Porcarelli, T. Rödlmeier, A. Sanchez-Sanchez, D. Mecerreyes, G. Hernandez-Sosa, *Adv. Funct. Mater.* **2018**, *28*, 1705795; d) H. Zheng, Y. N. Zheng, N. L. Liu, N. Ai, Q. Wang, S. Wu, J. H. Zhou, D. G. Hu, S. F. Yu, S. H. Han, W. Xu, C. Luo, Y. H. Meng, Z. X. Jiang, Y. W. Chen, D. Y. Li, F. Huang, J. Wang, J. B. Peng, Y. Cao, *Nat. Commun.* **2013**, *4*, 1971; e) Y. Zhou, C. Fuentes-Hernandez, J. Shim, J. Meyer, A. J. Giordano, H. Li, P. Winget, T. Papadopoulos, H. Cheun, J. Kim, M. Fenoll, A. Dindar, W. Haske, E. Najafabadi, T. M. Khan, H. Sojoudi, S. Barlow, S. Graham, J. L. Bredas, S. R. Marder, A. Kahn, B. Kippelen, *Science* **2012**, *336*, 327.

[10] a) J. Hwang, H. Kang, J.-E. Jeong, H. Y. Woo, M. J. Cho, S. Park, D. H. Choi, *Chem. Eng. J.* **2021**, *416*, 129185; b) T. Xu, X. Liang, G. Xie, *Front Chem* **2021**, *9*, 691172; c) J. Liu, L. Chen, X. Wang, Q. Yang, L. Zhao, C. Tong, S. Wang, S. Shao, L. Wang, *Macromol. Rapid Commun.* **2022**, *43*, 2200079; d) S. Xu, Q. Yang, Y. Zhang, H. Li, Q. Xue, G. Xie, M. Gu, J. Jin, L. Huang, R. Chen, *Chin. Chem. Lett.* **2021**, *32*, 1372; e) N. Ikeda, S. Oda, R. Matsumoto, M. Yoshioka, D. Fukushima, K. Yoshiura, N. Yasuda, T. Hatakeyama, *Adv. Mater.* **2020**, *32*, 2004072; f) F. Chen, L. Zhao, X. Wang, Q. Yang, W. Li, H. Tian, S. Shao, L. Wang, X. Jing, F. Wang, *Sci. China: Chem.* **2021**, *64*, 547; g) T. Wang, Y. Zou, Z. Huang, N. Li, J. Miao, C. Yang, *Angew. Chem., Int. Ed.* **2022**, *61*, e202211172.

[11] a) Q. Pei, G. Yu, C. Zhang, Y. Yang, A. J. Heeger, *Science* **1995**, *269*, 1086; b) J. D. Slinker, C. Y. Koh, G. G. Malliaras, M. S. Lowry, S. Bernhard, *Appl. Phys. Lett.* **2005**, *86*, 173506.

[12] a) A. Sandström, H. F. Dam, F. C. Krebs, L. Edman, *Nat. Commun.* **2012**, *3*, 1002; b) A. Sandström, A. Asadpoordarvish, J. Enevold, L. Edman, *Adv. Mater.* **2014**, *26*, 4975; c) Z. Zhang, K. Guo, Y. Li, X. Li, G. Guan, H. Li, Y. Luo, F. Zhao, Q. Zhang, B. Wei, Q. Pei, H. Peng, *Nat. Photon.* **2015**, *9*, 233; d) Z. Zhang, Q. Zhang, K. Guo, Y. Li, X. Li, L. Wang, Y. Luo, H. Li, Y. Zhang, G. Guan, B. Wei, X. Zhu, H. Peng, *J. Mater. Chem. C* **2015**, *3*, 5621; e) T. Lanz, A. Sandström, S. Tang, P. Chabrecek, U. Sonderegger, L. Edman, *Flexible Printed Electron.* **2016**, *1*, 025004; f) E. M. Lindh, A. Sandstrom, M. R. Andersson, L. Edman, *Light Sci Appl* **2016**, *5*, e16050; g) K. Sato, S. Uchida, S. Toriyama, S. Nishimura, K. Oyaizu, H. Nishide, Y. Nishikitani, *Adv. Mater. Technol.* **2017**, *2*, 1600293; h) J. Zimmermann, S. Schlisske, M. Held, J.-N. Tisserant, L. Porcarelli, A. Sanchez-Sanchez, D. Mecerreyes, G. Hernandez-Sosa, *Adv. Mater. Technol.* **2019**, *4*, 1800641; i) L. Mardegan, A. Paliwal, K. P. S. Zanoni, D. Tordera, H. J. Bolink, *Adv. Opt. Mater.* **2022**, *10*, 2201953.

[13] P. Matyba, K. Maturova, M. Kemerink, N. D. Robinson, L. Edman, *Nat. Mater.* **2009**, *8*, 672.

[14] a) L. M. Cavinato, K. Yamaoka, S. Lipinski, V. Calvi, D. Wehenkel, R. van Rijn, K. Albrecht, R. D. Costa, *Adv. Funct. Mater.* **2023**. https://doi.org/10.1002/adfm.202302483; b) X. J. Chen, Y. T. Huang, D. Luo, C. H. Chang, C. W. Lu, H. C. Su, *Chemistry* **2023**, *29*, 202300034; c) S. Uchida, Y. Nishikitani, *Adv. Funct. Mater.* **2020**, *30*, 1907309; d) J. C. Ye, Y. He, K. F. Li, L. H. Liu, C. Y. Xi, Z. B. Liu, Y. M. Ma, B. H. Zhang, Y. Bao, W. Wang, Y. X. Cheng, L. Niu, *ACS Appl. Mater. Interfaces* **2022**, *14*, 17698; e) P. Lundberg, E. M. Lindh, S. Tang, L. Edman, *ACS Appl. Mater. Interfaces* **2017**, *9*, 28810; f) P. Lundberg, Y. Tsuchiya, E. M. Lindh, S. Tang, C. Adachi, L. Edman, *Nat. Commun.* **2019**, *10*, 5307; g) C. E. Housecroft, E. C. Constable, *J. Mater. Chem. C* **2022**, *10*, 4456; h) S. Tang, P. Lundberg, Y. Tsuchiya, J. Ràfols-Ribé, Y. Liu, J. Wang, C. Adachi, L. Edman, *Adv. Funct. Mater.* **2022**, *32*, 2205967; i) R. Y. Yu, Y. J. Song, K. Zhang, X. C. Pang, M. X. Tian, L. He, *Adv. Funct. Mater.* **2022**, *32*, 2110623.

[15] D. Hall, S. M. Suresh, P. L. dos Santos, E. Duda, S. Bagnich, A. Pershin, P. Rajamalli, D. B. Cordes, A. M. Z. Slawin, D. Beljonne, A. Köhler, I. D. W. Samuel, Y. Olivier, E. Zysman-Colman, *Adv. Opt. Mater.* **2020**, *8*, 1901627.

[16] M. Karaman, A. K. Gupta, S. M. Suresh, T. Matulaitis, L. Mardegan, D. Tordera, H. J. Bolink, S. Wu, S. Warriner, I. D. Samuel, E. Zysman-Colman, *Beilstein J. Org. Chem.* **2022**, *18*, 1311.

[17] Y. Xu, Z. Cheng, Z. Li, B. Liang, J. Wang, J. Wei, Z. Zhang, Y. Wang, *Adv. Opt. Mater.* **2020**, *8*, 1902142.

[18] a) S. A. Jenekhe, J. A. Osaheni, *Science* **1994**, *265*, 765; b) G. v. Bünau, *Berichte der Bunsengesellschaft für physikalische Chemie* **1970**, *74*, 1294.

[19] a) K. S. Son, M. Yahiro, T. Imai, H. Yoshizaki, C. Adachi, *Chem. Mater.* **2008**, *20*, 4439; b) S.-J. Su, C. Cai, J. Kido, *Chem. Mater.* **2011**, *23*, 274.

[20] E. Zysman-Colman, *Nat. Photonics* **2020**, *14*, 593.

[21] P. Lundberg, Q. Wei, Z. Ge, B. Voit, S. Reineke, L. Edman, *J. Phys. Chem. Lett.* **2020**, *11*, 6227.

[22] a) M. Diethelm, A. Schiller, M. Kawecki, A. Devižis, B. Blülle, S. Jenatsch, E. Knapp, Q. Grossmann, B. Ruhstaller, F. Nüesch, R. Hany, *Adv. Funct. Mater.* **2020**, *30*, 1906803; b) S. Tang, A. Sandström, P. Lundberg, T. Lanz, C. Larsen, S. van Reenen, M. Kemerink, L. Edman, *Nat. Commun.* **2017**, *8*, 1190.

[23] J. Ràfols-Ribé, X. Zhang, C. Larsen, P. Lundberg, E. M. Lindh, C. T. Mai, J. Mindemark, E. Gracia-Espino, L. Edman, *Adv. Mater.* **2022**, *34*, 2107849.

[24] a) Q. Pei, Yang, G. Y.u, C. Zhang, A. J. Heeger, *J. Am. Chem. Soc.* **1996**, *118*, 3922; b) S. B. Meier, S. van Reenen, B. Lefevre, D. Hartmann, H. J. Bolink, A. Winnacker, W. Sarfert, M. Kemerink, *Adv. Funct. Mater.* **2013**, *23*, 3531; c) M. Lenes, G. Garcia-Belmonte, D. Tordera, A. Pertegas, J. Bisquert, H. J. Bolink, *Adv. Funct. Mater.* **2011**, *21*, 1581.

[25] S. Tang, Z. Wang, Y. Xu, H. Ma, J. Wang, C. Larsen, D. Dang, E. Wang, L. Edman, *Angew. Chem., Int. Ed.* **2023**, *62*, e202302874.

[26] J. Mindemark, L. Edman, *J. Mater. Chem. C* **2016**, *4*, 420.

[27] J. Rafols-Ribe, E. Gracia-Espino, S. Jenatsch, P. Lundberg, A. Sandstrom, S. Tang, C. Larsen, L. Edman, *Adv. Opt. Mater.* **2021**, *9*, 2001405.

[28] a) F. A. Meltem, M. D. P. Bianka, T. Yu, B. Thomas, S. U. Alexander, D. C. Rubén, D. Pablo, *J. Phys. D: Appl. Phys.* **2018**, *51*, 334001; b) G. Qian, Y. Lin, G. Wantz, A. R. Davis, K. R. Carter, J. J. Watkins, *Adv. Funct. Mater.* **2014**, *24*, 4484; c) A. Mishra, R. Bose, Y. Zheng, W. Xu, R. McMullen, A. B. Mehta, M. J. Kim, J. W. P. Hsu, A. V.

Malko, J. D. Slinker, *Adv. Mater.* **2022**, *34*, 2203226; d) Y.-H. Su, Y.-C. Ji, Y.-T. Huang, D. Luo, S.-W. Liu, Z.-P. Yang, C.-W. Lu, C.-H. Chang, H.-C. Su, *J. Mater. Chem. C* **2022**, *10*, 18137; e) Y. Liu, S. Tang, X. Wu, N. Boulanger, E. Gracia-Espino, T. Wågberg, L. Edman, J. Wang, *Nano Res.* **2022**, *15*, 5610; f) Y.-C. Chiu, R.-H. Yi, T.-Y. Ou, D. Luo, J.-Y. Lien, Z.-P. Yang, C.-W. Lu, H.-C. Su, *Org. Electron.* **2021**, *88*, 106016; g) A. J. Norell Bader, A. A. Ilkevich, I. V. Kosilkin, J. M. Leger, *Nano Lett.* **2011**, *11*, 461; h) A. Mishra, S. DiLuzio, M. Alahbakhshi, A. C. Adams, M. H. Bowler, J. Moon, Q. Gu, A. A. Zakhidov, S. Bernhard, J. D. Slinker, *Chem. Mater.* **2021**, *33*, 1201.

[29] A. Mishra, M. Alahbakhshi, R. Haroldson, Q. Gu, A. A. Zakhidov, J. D. Slinker, *Adv. Funct. Mater.* **2021**, *31*, 2102006.

[30] Y. Qi, X. Cao, Y. Zou, C. Yang, *J. Mater. Chem. C* **2021**, *9*, 1567.